

Observations of regional phase propagation across the Tibetan Plateau

Daniel E. McNamara¹ and Thomas J. Owens

Department of Geological Sciences, University of South Carolina, Columbia

William R. Walter

Earth Sciences Division, Lawrence Livermore National Laboratory, Livermore, California

Abstract. We present observations of regional phase velocity and propagation characteristics using data recorded during a 1-year deployment of broadband digital seismic stations across the central Tibetan Plateau along the Qinghai-Tibet highway from Golmud to Lhasa. Previous seismological studies within this region have had to rely on earthquakes recorded almost exclusively at stations outside of the plateau. We have the opportunity to study numerous source-receiver paths confined entirely within the Tibetan Plateau. Our analysis concentrates on travel time, amplitude, and frequency content measurements of the *Pg*, *Pn*, and *Sn* phases. *Pn* can be clearly picked for all observed paths and propagates at an average velocity of 8.16 ± 0.07 km/s within the Tibetan Plateau. *Sn*, however, shows dramatic variations in propagation efficiency across the Tibetan Plateau that is strongly dependent on frequency. We observe that *Sn* rapidly decreases in frequency and amplitude as it passes through the northern portion of the plateau. We show that in general, *Sn* propagation efficiency decreases with increasing frequency content. We use 122 events from outside of the plateau and 61 from within to refine the boundaries of a region of inefficient high-frequency *Sn* propagation. Specifically, we show that a larger portion of the northern Tibetan Plateau attenuates *Sn* energy than was previously suggested. In the southern plateau, where high-frequency *Sn* is observed, we computed an average velocity of 4.59 ± 0.18 km/s. We also observed that the *Pn* velocity within this region of inefficient high-frequency *Sn* propagation is nearly 4% slower than the *Pn* velocity computed for paths restricted to the southern plateau and that the crust is about 10 km thinner than in the south. The coincident locations of inefficient *Sn* propagation and slow *Pn* velocity is commonly observed in regions of active tectonics. Our results add constraints to the velocity structure of the lithosphere beneath the Tibetan Plateau and require first-order lateral variations in the uppermost mantle structure, despite the relatively uniform topography of the plateau.

Introduction

We summarize observations of seismic velocity and propagation characteristics for the regional phases (*Pg*, *Pn*, and *Sn*) recorded at 11 three-component, broadband, digital seismic stations across the central Tibetan Plateau (Figure 1 and Table 1). The primary goals of this study are to determine phase velocities for *Pg*, *Pn*, and *Sn* and to map the lateral variation in amplitude and frequency of *Sn* within the Tibetan Plateau. Regional phases, such as *Sn* and *Pn*, propagate within the mantle component of the lithosphere. Propagation information from these phases can be used to infer velocity structure of the mantle lid. The mantle lid is thought to have an important role in the evolution of the Tibetan Plateau. Additional velocity constraints will aid in our understanding of this important continental collision.

¹Now at Earth Sciences Division, Lawrence Livermore National Laboratory, Livermore, California.

Copyright 1995 by the American Geophysical Union.

Paper number 95JB01863.
0148-0227/95/95JB-01863\$05.00

During 1 year of recording (July 1991 to July 1992) 183 events, at regional distances to our array (3° - 16°), were recorded. Sixty-one of these events were located within the Tibetan Plateau (Figure 1 and Table 2) offering a unique opportunity to observe seismic phases that both originated and propagated entirely within the Tibetan Plateau. Previous studies using regional Tibetan Plateau earthquakes have placed first-order constraints on upper mantle velocity structure but have had to rely on data recorded almost exclusively at stations outside of the plateau. With our pure path data set, we avoid propagation effects due to interaction with the boundaries of the plateau and obtain regional phase velocity estimates and amplitude measurements as a function of frequency that reflect the properties of the Tibetan Plateau.

The Tibetan Plateau has intrigued geoscientists for both its impressive physiographic features as well as its geographic remoteness. The remoteness of the plateau has led to a relative lack of data available for interpretation. Consequently, this important continental collision is poorly understood. It is known that the Tibetan Plateau is composed of a series of tectonic terranes that accreted onto the southern margin of Eurasia after the breakup of Gondwana. Since the collision of India with Eurasia, about 40 my ago, nearly 2000 km of convergence has occurred giving rise to the Himalaya and Karakoram ranges

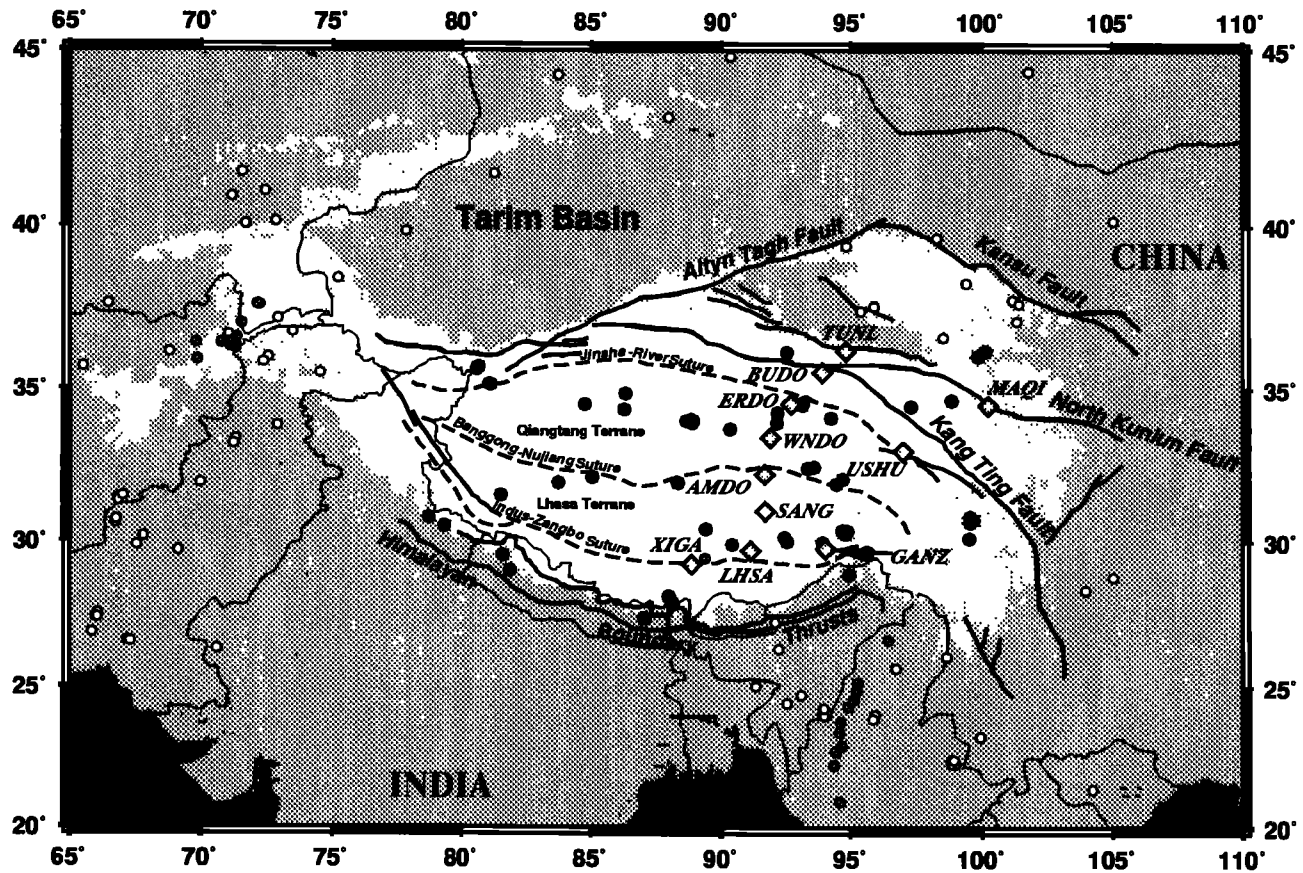


Figure 1. Tibetan Plateau experiment base map showing recording stations (light grey diamonds) and the distribution of 61 Tibetan Plateau regional events (solid circles) recorded during the 1 year of deployment. Additional events (open circles), outside of the 3000-m contour, are used to analyze S_n propagation across the boundaries of the plateau. Elevation is shown with grey scales. The open region is above 4000 m, light grey region is between 3000 m and 4000 m, and the large dark grey region is less than 3000 m above sea level. Regional structural trends are taken from Dewey *et al.* [1988]. Major faults are shown as solid lines, and tectonic terrane sutures are shown as dashed lines. Intermediate depth earthquakes (70-250 km) are shown as grey circles.

as well as the Tibetan Plateau [Harrison *et al.*, 1992]. The Tibetan Plateau stands out because of its high, uniform elevation (5000 m) and its anomalously thick crust (65-70 km) [Molnar, 1988]. To date, the paucity of interpretable data has not allowed for the determination of the exact tectonic mechanism that produced the Tibetan Plateau. This has led to a wide variety of tectonic models, most of which fall into two basic end-member theories. One model attributes crustal thickening and lithospheric shortening to compression generated from the continental collision between the Indian and Eurasian plates [Dewey and Burke, 1973]. A second model suggests that uplift occurred by shallow underthrusting of the Indian lithosphere beneath Eurasia during collision [Argand, 1924; Barazangi and Ni, 1982; Beghoul *et al.*, 1993].

Many first-order geological and geophysical observations have been made (for review, see Molnar [1988]), but information about the mantle velocity structure remains ambiguous. Previous studies, using regional phases, have been conducted with stations outside the plateau, with the exception of one station located near Lhasa, and have reported a wide range of P_n velocities. The lowest average P_n velocity reported for the Tibetan Plateau is 7.93 ± 0.17 km/s [Zhao and Xie, 1993]. Other estimates report P_n and S_n velocities of 8.1 km/s and 4.7 km/s

respectively [Chen and Molnar, 1981; Jia *et al.*, 1981; Ding *et al.*, 1993]. Still other studies have found significantly higher velocities for P_n and S_n (8.43 km/s and 4.73 km/s) [Barazangi and Ni, 1982; Ni and Barazangi, 1983; Beghoul *et al.*, 1993]. The disparate results of these separate studies allowed their authors to favor opposing theories for the evolution of the Tibetan Plateau. In general, low P_n velocity is cited in sup-

Table 1. Tibetan Plateau Seismic Experiment Station Locations

Station	Latitude N°	Longitude E°	Elevation (m)
AMDO	32.247	91.688	4712
BUDO	35.529	93.910	4660
ERDO	34.520	92.707	4623
GANZ	29.767	94.050	3150
LHASA	29.702	91.128	3700
SANG	31.024	91.700	4740
TUNL	36.199	94.815	3133
WUNDO	33.448	91.904	4865
XIGA	29.234	88.851	3865
MAQI	34.478	100.249	3823
USHU	33.011	97.015	3727

Table 2. Tibetan Plateau Experiment Regional Events

Event ID†	Origin Time‡	Latitude °N	Longitude °E	Depth, km	m_b	Number of Stations
91.193.21.55.49	91193220600.2	39.421	94.832	16	4.8	4
91.199.09.53.55	91199095036.7	8.224	94.112	27	5.4	5
91.199.13.23.31	91199132459.9	30.363	94.870	33	5.0	9
91.199.15.27.32	91199152405.1	8.439	94.629	16	5.1	1
91.199.17.44.50	91199174543.5	30.362	94.667	33	4.2	6
91.201.18.52.00	91201185223.9	30.298	94.741	33	4.5	7
91.201.18.52.05	91201190230.6	30.326	94.838	24	4.8	9
91.204.13.29.37	91204132547.3	3.775	95.932	47	5.8	8
91.204.16.50.24	91204165154.0	30.269	94.820	33	4.7	9
91.205.06.06.43	91205060644.5	30.302	94.785	33	4.8	7
91.206.01.52.18	91206015245.2	30.317	94.791	33	4.8	7
91.209.23.57.54	91209235820.2	30.329	94.793	33	4.9	8
91.210.03.18.45	91210032015.6	30.294	94.765	33	4.6	5
91.210.15.47.13	91210154808.8	30.269	94.793	33	4.7	9
91.211.22.21.39	91211222205.9	30.385	94.795	33	4.8	8
91.215.08.38.02	91215083317.1	29.330	129.081	17	5.5	2
91.216.12.42.55	91216123824.5	23.888	95.859	43	4.7	8
91.218.02.21.24	91218021731.6	3.827	95.374	18	6.0	6
91.220.11.15.33	91220111238.4	26.879	65.848	53	5.3	10
91.222.20.21.24	91222202151.7	33.910	92.158	10	4.7	11
91.231.06.07.09	91231060551.3	46.944	85.302	30	5.5	8
91.234.03.53.11	91234035341.1	25.030	91.330	33	4.7	9
91.234.21.26.07	91234211504.5	55.771	114.364	23	5.2	1
91.235.07.39.13	91235073625.8	36.155	68.802	33	4.9	5
91.236.17.46.43	91236174523.3	38.441	75.213	33	4.7	4
91.237.05.04.30	91237050059.8	5.649	94.116	44	5.2	7
91.238.20.45.55	91238204231.8	6.937	94.531	26	5.4	9
91.238.20.54.25	91238205423.0	6.882	94.609	22	5.8	8
91.239.05.14.10	91239051432.3	34.249	92.161	33	3.4	9
91.242.14.30.58	91242143212.8	34.449	97.309	33	4.3	8
91.245.11.05.48	91245110550.4	37.440	95.402	10	5.5	11
91.247.08.35.12	91247083233.5	10.746	92.843	33	5.1	8
91.247.22.31.26	91247222721.7	15.204	120.404	21	5.6	3
91.250.03.00.10	91250030024.3	24.252	93.976	33	4.9	7
91.251.23.53.44	91251235441.5	36.626	98.553	23	4.8	8
91.252.21.54.32	91252215450.5	28.879	94.937	33	4.8	11
91.255.00.45.09	91255003330.7	54.905	111.112	25	5.1	3
91.255.23.05.10	91255230630.1	29.698	95.688	34	4.6	7
91.257.13.17.47	91257131639.7	40.171	105.046	25	5.1	10
91.258.00.23.59	91258002050.3	30.617	66.735	33	4.8	5
91.258.02.15.33	91258021224.9	30.724	66.763	26	4.6	5
91.260.18.53.51	91260185322.2	43.141	87.968	22	4.8	4
91.262.04.23.29	91262042356.7	26.323	92.211	33	4.7	6
91.263.09.41.20	91263093742.5	44.832	90.332	33	4.8	2
91.263.11.15.36	91263111611.5	36.191	100.063	13	5.5	10
91.265.05.45.35	91265054227.8	30.165	67.799	10	4.9	1
91.270.07.39.55	91270073955.3	34.645	98.874	33	4.7	7
91.270.11.55.24	91270115640.8	29.911	90.423	33	3.7	5
91.270.23.29.56	91270233121.4	32.444	93.354	33	4.3	8
91.273.09.47.58	91273094442.1	22.535	121.479	24	5.5	7
91.273.16.33.41	91273163306.2	37.766	101.323	20	5.3	11
91.273.18.35.45	91273183544.2	22.728	94.416	75	4.7	10
91.274.20.33.26	91274203020.0	35.705	65.512	12	5.3	10
91.279.10.58.20	91279105044.4	21.384	104.231	10	4.5	3
91.279.12.16.45	91279121812.0	37.677	101.437	10	4.1	3
91.285.05.12.00	91285050836.3	22.798	121.536	8	5.1	3
91.285.12.23.03	91285122347.2	37.791	101.176	36	4.3	5
91.288.19.11.31	91288191100.9	30.565	79.311	33	4.5	2
91.292.21.24.47	91292212314.3	30.780	78.774	10	6.5	11
91.293.05.34.33	91293053226.8	30.790	78.686	27	4.9	2
91.296.20.41.02	91296203709.1	20.836	122.158	29	4.4	2
91.298.14.44.00	91298144039.8	23.788	122.952	27	5.2	3
91.304.02.31.18	91304022902.5	40.148	72.841	21	5.2	10
91.307.00.03.04	91307000225.9	28.365	103.984	33	4.5	2
91.312.15.16.59	91312151344.1	26.323	70.607	22	5.6	11

Table 2. (continued)

Event ID†	Origin Time‡	Latitude °N	Longitude °E	Depth, km	m_b	Number of Stations
91.319.19.56.36	91319195343.5	29.696	69.134	19	4.6	6
91.320.12.17.40	91320121422.5	37.660	66.469	33	4.8	3
91.323.01.03.09	91323010418.0	32.484	93.593	33	4.9	10
91.325.13.36.25	91325133742.1	33.714	90.337	33	4.3	9
91.328.07.34.25	91328073526.6	33.980	88.646	33	4.7	8
91.329.10.07.40	91329100839.0	34.017	88.832	33	4.4	9
91.330.15.30.17	91330153114.7	33.919	88.746	33	4.1	8
91.330.21.15.51	91330211559.9	34.073	94.247	33	4.3	10
91.336.19.44.36	91336194536.6	32.090	94.694	46	4.4	9
91.337.13.19.49	91337131644.1	9.095	92.470	37	4.7	4
91.338.03.27.07	91338032724.2	24.015	93.986	72	4.9	11
91.339.15.51.42	91339154820.7	22.544	121.450	17	4.6	3
91.341.13.57.39	91341135740.6	24.059	93.913	69	5.1	11
91.341.14.26.09	91341142232.2	25.191	62.974	30	5.2	4
91.343.01.03.52	91343010246.5	29.543	81.632	29	5.6	11
91.348.08.19.24	91348082023.8	33.976	88.840	33	5.1	8
91.349.15.58.26	91349155932.8	29.970	93.928	33	4.8	9
91.351.20.26.50	91351202749.6	33.990	88.904	33	4.6	9
91.351.23.51.10	91351234954.5	44.333	83.727	17	4.9	5
91.353.18.59.32	91353185517.4	28.102	57.304	27	5.3	3
91.354.02.05.53	91354020605.3	24.720	93.103	41	5.3	10
91.355.19.52.42	91355195245.5	27.904	88.139	57	4.9	9
91.357.01.57.23	91357015825.1	33.917	88.863	33	5.2	8
91.357.02.14.54	91357021454.5	33.966	88.942	33	5.0	9
91.358.21.26.32	91358212752.1	30.003	92.544	33	4.4	6
91.359.12.16.26	91359121322.3	10.607	93.906	40	4.7	6
91.360.13.26.42	91360132417.7	30.837	99.532	33	4.1	5
91.361.09.11.27	91361090937.5	51.019	98.150	14	5.8	10
91.362.09.14.39	91362090703.3	51.096	98.061	17	5.0	5
91.365.21.13.33	91365211418.5	30.657	99.571	33	4.5	8
92.002.02.34.36	92002023537.2	33.990	88.859	33	4.8	9
92.004.03.37.35	92004033521.6	31.954	69.991	29	5.0	9
92.005.17.23.27	92005171421.0	40.873	71.172	16	5.0	2
92.005.17.30.00	92005172319.8	41.583	71.556	33	4.4	2
92.007.16.23.40	92007162309.9	30.118	99.537	36	4.8	8
92.008.17.40.21	92008174141.5	30.137	92.449	33	4.0	5
92.011.06.19.51	92011061655.9	9.311	86.964	22	5.7	8
92.012.00.11.55	92012001227.1	39.671	98.300	22	5.4	6
92.013.18.36.22	92013183632.1	24.439	92.557	33	4.5	5
92.020.09.01.16	92020085822.5	27.398	65.994	27	5.2	7
92.021.22.10.43	92021220758.9	26.632	67.198	26	5.4	8
92.022.21.43.49	92022214125.9	35.351	121.109	33	5.1	6
92.023.10.25.28	92023102626.7	34.566	93.164	33	5.2	5
92.024.05.06.18	92024050447.3	35.515	74.529	47	5.4	6
92.025.15.16.29	92025151231.9	26.070	98.668	33	4.7	1
92.030.05.25.29	92030052201.4	24.958	63.141	29	5.5	3
92.034.15.43.19	92034154422.6	34.496	93.147	10	4.7	6
92.036.11.04.57	92036105713.0	50.260	100.168	45	4.4	1
92.036.19.42.54	92036193629.8	31.513	67.038	33	4.4	1
92.036.23.13.35	92036231048.6	31.426	66.825	18	5.1	6
92.036.23.43.40	92036234136.8	31.365	66.858	33	5.0	4
92.037.03.34.31	92037033515.3	29.610	95.521	15	5.6	6
92.040.12.44.12	92040124452.7	29.627	95.646	10	5.1	6
92.040.14.36.56	92040143734.7	29.660	95.607	10	4.8	2
92.041.12.42.34	92041123857.1	21.173	121.901	22	5.0	2
92.045.08.21.20	92045081825.7	53.897	108.866	21	5.3	3
92.054.20.07.30	92054200625.2	41.556	81.267	33	4.7	1
92.065.02.15.19	92065021417.6	35.625	80.585	36	4.7	3
92.067.06.31.49	92067062855.3	40.075	71.685	25	4.9	3
92.069.17.02.51	92069165928.6	27.424	66.044	19	4.9	7
92.075.01.05.37	92075010127.1	23.548	123.562	31	5.7	8
92.076.01.18.29	92076011855.9	34.343	86.288	33	4.7	6
92.077.02.17.41	92077021449.6	9.216	92.833	67	4.8	8
92.079.06.38.32	92079063425.8	17.155	120.827	15	5.7	4
92.082.01.51.00	92082014755.0	10.553	93.904	33	4.9	5

Table 2. (continued)

Event ID†	Origin Time‡	Latitude °N	Longitude °E	Depth, km	m_b	Number of Stations
92.084.19.32.48	92084193210.3	31.545	81.540	16	4.8	3
92.084.21.04.01	92084210147.5	33.832	72.905	14	5.0	9
92.085.17.19.11	92085171537.6	24.455	123.318	78	5.4	3
92.087.10.41.40	92087103930.6	35.997	72.548	35	4.9	7
92.088.10.20.59	92088101741.8	26.582	67.303	10	4.9	6
92.090.18.27.39	92090183006.6	31.929	94.465	33	3.9	9
92.090.19.22.19	92090191934.8	35.855	72.374	55	4.4	1
92.092.13.40.48	92092134103.9	27.392	87.065	33	4.3	4
92.092.20.54.29	92092205403.7	31.964	83.754	52	4.1	3
92.095.17.42.50	92095174320.7	28.147	87.979	33	4.9	9
92.096.07.47.27	92096074747.6	35.696	80.661	18	5.5	9
92.096.11.08.11	92096110923.1	35.665	80.599	33	4.0	2
92.097.19.49.55	92097194911.3	44.427	101.792	33	4.7	2
92.103.18.41.18	92103183716.5	29.515	131.396	39	5.6	1
92.104.03.46.58	92104034751.0	31.958	88.339	33	4.6	9
92.109.18.19.52	92109181929.2	36.155	92.538	10	4.1	9
92.110.18.35.29	92110183219.0	23.861	121.594	16	5.8	1
92.111.18.49.38	92111185028.3	27.256	92.077	33	4.6	7
92.114.12.25.22	92114122117.2	29.429	131.364	40	5.8	1
92.114.14.19.00	92114141835.1	22.437	98.904	12	5.8	10
92.114.15.33.13	92114153249.1	22.418	98.852	10	5.9	10
92.114.17.20.05	92114171502.7	22.309	98.856	33	4.7	8
92.114.18.24.18	92114181811.6	22.303	98.997	33	4.8	7
92.115.07.10.45	92115070723.9	27.550	66.065	25	5.9	9
92.115.12.04.17	92115114912.3	23.768	121.660	18	4.7	2
92.119.01.36.25	92119013628.9	32.145	85.066	33	3.8	4
92.119.21.08.48	92119210303.6	22.430	98.935	33	4.6	3
92.122.08.10.36	92122080945.0	19.583	94.419	55	4.6	4
92.125.10.57.33	92125105422.2	29.882	67.550	10	4.9	5
92.130.07.23.48	92130072344.8	34.503	84.774	10	4.6	3
92.131.04.06.36	92131040432.9	37.207	72.913	33	5.6	9
92.132.11.21.35	92132112341.4	36.794	73.487	33	4.7	2
92.136.08.10.26	92136080802.9	41.019	72.429	50	5.7	6
92.137.08.34.31	92137083257.7	23.262	99.939	33	4.6	2
92.137.20.20.20	92137201952.9	36.080	99.869	17	5.0	8
92.139.19.55.16	92139195538.8	34.858	86.331	33	4.1	6
92.141.12.22.51	92141122032.8	33.377	71.317	16	6.0	9
92.142.05.00.01	92142045957.5	41.604	88.813	00	6.5	8
92.143.05.46.46	92143054731.5	30.748	99.685	33	4.6	6
92.146.05.10.38	92146050813.1	36.701	71.046	48	4.9	6
92.147.19.00.39	92147185654.8	20.100	121.396	53	4.9	1
92.154.22.08.09	92154220745.3	28.984	81.913	56	5.2	9
92.155.01.59.24	92155015513.3	28.083	128.094	56	4.9	1
92.155.02.41.37	92155024236.6	33.905	88.893	10	4.6	7
92.157.00.26.01	92157002343.7	33.241	71.228	33	4.9	6
92.162.13.41.31	92162134124.9	25.660	96.758	33	4.7	5
92.165.16.56.33	92165165507.7	39.845	77.828	35	4.7	3
92.167.02.49.28	92167024856.2	24.027	95.932	17	5.8	5
92.173.08.07.07	92173080746.5	30.428	89.394	28	4.2	2
92.173.11.11.02	92173111939.7	38.307	99.423	20	4.8	3
92.179.02.14.16	92179021318.3	35.148	81.079	33	4.5	4
92.179.13.22.17	92179132120.9	35.139	81.131	33	5.0	4

† Based on the notation of *Owens et al.* [1993b].

‡ Origin time in year, day, hours, minutes, and seconds.

port of lithospheric shortening models while faster Pn velocities are explained by models involving continental underthrust.

Data

We measure arrival times using data digitally recorded from broadband Streckeisen STS-2 sensors at 11 sites within the central portion of the Tibetan Plateau [*Owens et al.*, 1993a and b].

Initial event locations were determined from the U.S. Geological Survey (USGS) monthly Preliminary Determination of Epicenters (PDE) catalog. Locations for a small subset of Tibetan Plateau events have been improved and will be discussed later. We define two distinct data sets based on epicentral location. First, we use 61 events with epicenters within the Tibetan Plateau for phase velocity calculations (Figure 1 and Table 2). For this data set only events with propagation paths within the

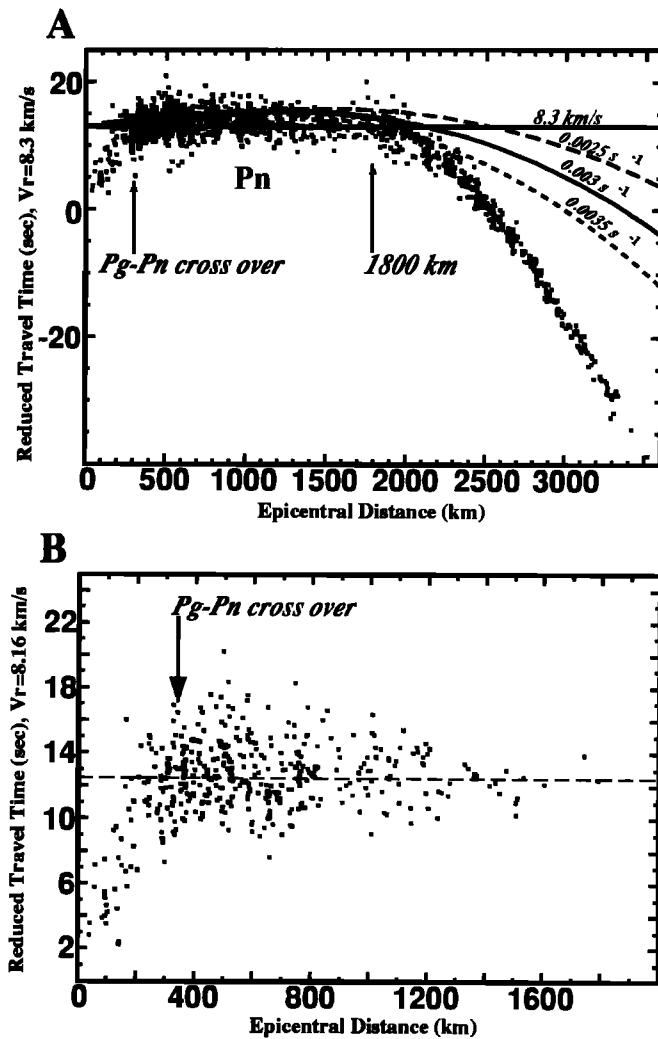


Figure 2. (a) Travel time picks for 1090 first arrivals, from 183 events, at regional distances to the array. This data set includes event/station paths that cross the plateau boundaries as well as paths from 61 events within the plateau. A reducing velocity of 8.3 km/s was used to highlight the Pg - Pn crossover distance and the distance where Pn is no longer the first arrival (~1800 km). Three separate travel time curves are shown for mantle lid velocity gradients of 0.0025, 0.003, and 0.0035 s^{-1} . (b) Travel time picks for first arrivals from 61 events within the Tibetan Plateau. These data are restricted to event/station paths confined to the Tibetan Plateau. Travel times are shown with a reducing velocity of 8.16 km/s. Pn travel time picks are shown as solid squares.

3000-m elevation contour are considered (Figure 1). Second, we use 122 additional events, with sources located outside of the plateau (Table 2), to evaluate the propagation characteristics of Sn and to place constraints of the Pn crossover distances (Table 2).

The phase, Pg , as used in our study is the direct compressional arrival that propagates at local distances within the crust. Previous authors have shown that Pg is the first arrival for epicentral distances less than approximately 3° (333 km) within the Tibetan Plateau [Beghoul *et al.*, 1993]. Beyond this distance Pg is observed as the second major arrival, behind the much smaller amplitude Pn . The regional crossover distance can be

seen as the first change in slope of the first arrival travel times versus distance (Figure 2a). Both Pn and Sn are regional distance refracted or shallow turning waves that travel in the high-velocity upper-mantle lid. Beyond 1800 km the first arrival is no longer Pn as the P -wave begins to interact with the sublithospheric mantle.

Observed Phase Velocities Within the Tibetan Plateau

Pn observations. Pn was picked as the first motion on the vertical component at regional distances to our array. To aid in picking, we examined broadband, high-pass-filtered (corner 1 Hz) and band-pass-filtered (corner 0.5-4 Hz) records as well as the envelopes of each passband. Pn arrival time was chosen as the earliest clear arrival of all passbands examined. In general, the high-frequency traces were best for picking accurate arrival times since Pn is emergent at longer periods and difficult to pick precisely. Examples of Pn are shown in the event record sections used later to illustrate Sn behavior (Figures 5-9). Because both a number of stations and events were used for velocity calculations, travel times were corrected for both focal depth and station elevation. Previously published crustal velocities [Beckers *et al.*, 1994] were used to compute the vertical slowness that was then multiplied by the deviation in station elevation or focal depth from the reference datum at sea level. When applied to the raw travel times, these corrections slightly reduced the scatter in our data.

Figure 2a shows 1090 corrected, first-arrival picks from all 183 events recorded at regional distances from our array. Pn is the first arrival and can be fit by a straight line between the regional Pg - Pn crossover distance out to 1800 km where deeper mantle P waves arrive before Pn . A velocity of 8.29 ± 0.18 km/s with an intercept time of 13.5 s was obtained by fitting travel times in the distance range where Pn is the first arrival on the seismogram. This is roughly consistent with the higher end Pn velocities previously reported for the plateau [Beghoul *et al.*, 1993; Ni and Barazangi, 1983]. The Pn - Pg observed crossover distance of about 300 km, is less than the approximately 333 km (3°) crossover distance observed in previous studies without pure path plateau data (Figure 2a). To avoid contamination by slower Pg arrivals on our plateau Pn estimate, we will use the larger crossover distance. Previous studies have reported evidence for an upper mantle velocity gradient beneath the Tibetan Plateau [Holt and Wallace, 1990; Beghoul *et al.*, 1993; Zhao and Xie, 1993]. Figure 2a shows the travel time curves expected for the range of possible velocity gradients along with our entire travel time data set. Pn arrivals are relatively linear, suggesting a weak to non-existent velocity gradient exists beneath the plateau. Scatter in our data restricts our ability to detect a weak gradient or distinguish between gradient variations.

To focus our study on the uppermost mantle exclusively beneath the Tibetan Plateau, we now restrict our analysis to paths that are both entirely confined to the plateau and between distances of 333-1777 km (3-16°). Applying this restriction to the data set left travel times from 371 Pn arrivals from the 61 plateau events. A velocity of 8.16 ± 0.07 km/s was obtained from the slope of the L2 fit to the travel time data, with an intercept of 12.47 ± 0.48 s. The Pn velocity obtained from paths restricted to the plateau is lower than that obtained from the entire regional data set, as well as lower than estimates obtained by including paths longer than 1800 km. The inter-

cept time and P_n velocity corresponds to a crustal thickness of approximately 65 km when an average crustal velocity of 6.4 km/s is assumed [Beckers *et al.*, 1994]. These results are comparable to crustal thickness estimates and the median range P_n velocity estimates from previously published studies [Molnar, 1988].

Residuals relative to the velocity fit to the travel time data vary considerably and are shown in Figure 2b. Some are as large as 10 s, but most are within $\pm 1-5$ s. Such wide scatter is indicative of either poor picks, inaccurate event locations, or laterally heterogeneous velocity structure within the lithosphere beneath the Tibetan Plateau. P_n is often emergent and difficult to pick precisely; however, in most cases a precision of at least 0.5 s was obtainable. For this reason, we considered larger residuals to be related to lateral velocity variations within the uppermost mantle and/or event mislocation errors.

Lateral P_n velocity variations. To test the idea that lateral variations in upper mantle structure has an effect on P_n velocity and may contribute to the relatively large travel time residuals that we observe, we have computed velocities for subsets of P_n paths within the plateau. The most significant observation is a 4% velocity variation across the plateau with northern paths slower than the south. A P_n velocity of 8.03 ± 0.12 km/s was computed for 94 paths that propagate within the plateau, north of 32°N latitude. For 51 paths, south of 32°N , the velocity of P_n is significantly higher (8.32 ± 0.1 km/s).

There is also a significant intercept time variation between the northern and southern plateau suggesting lateral crustal thickness variations. We have not observed similar lateral variation of the crustal velocity from the P_g phase. For this reason we assume an average crustal velocity of 6.4 km/s across the plateau for crustal thickness estimates. An intercept of 10.8 ± 1.30 s corresponds to an average crustal thickness of approximately 57 km in the north, while the southern plateau intercept time of 13.9 ± 1.12 s corresponds to an average crustal thickness of about 69 km. Brandon and Romanowicz [1986] and Molnar [1988] report a 10-km thinning of the crust from south to north that is within the uncertainty of our results. Based on this information, lateral crustal thickness and P_n velocity variations within the uppermost mantle contribute to the relatively large travel time residuals that we observe. In a later section, we describe further attempts to reduce residuals by improving event locations.

S_n observations. Ni and Barazangi [1983] observed that high-frequency S_n energy is severely attenuated for paths that cross the north central portion of the plateau. Our data confirm this, and consequently, we were able to pick only 36 clear S_n arrivals from our high-frequency data set of Tibetan Plateau events. Observable S_n arrivals are restricted to paths within the southern plateau and propagate at an average velocity of 4.59 ± 0.18 km/s with an intercept of 24.02 ± 3.3 s. Uncertainty in our estimate is quite high due to the paucity of S_n observations; however, previous S_n velocity estimates for the Tibetan Plateau (4.7 km/s) are within two standard deviations of our observation [Chen and Molnar, 1981; Beghoul *et al.*, 1993; Ni and Barazangi, 1983]. Attempts were made to determine S_n velocity at longer periods; however, at long periods, S_n could not be picked precisely enough to calculate an accurate velocity.

P_g observations. To be consistent with the crustal thickness determined with an average intercept of 12.47 s and a P_n velocity of 8.16 km/s, the P_g - P_n crossover distance should occur at about 360 km. Since scatter of the travel time data is high at

the crossover, the P_g phase velocity was estimated at different distances. For paths out to 360 km, we compute a P_g velocity of 6.45 ± 0.22 km/s. If we use the previously observed crossover distance and fit all initial arrivals less than 333 km (3°), we compute a high P_g velocity of 6.4 ± 0.24 km/s. When the distance range is decreased to 0-300 km, P_g velocity decreases to 6.38 ± 0.25 km/s. P_g velocities at these three distance ranges are relatively consistent. Velocity significantly increases to 6.75 km/s when paths as long as 380 km are included. Contamination by faster P_n arrivals beyond the actual crossover distance will bias P_g velocity estimates toward higher values. This suggests that the crossover distance is likely between 300 and 360 km. This distance range roughly coincides with expected crossover distances within the range of our intercept time uncertainty. At small epicentral distances, event depth and location errors cause relatively larger percent error than at greater distances. For these reasons, we cannot more accurately define the P_g - P_n crossover distance.

Event Relocation

Event locations and focal depths reported by the USGS PDE catalogs have been shown to be in error by as much as 25 km within the Tibetan Plateau [Zhao and Helmlinger, 1991]. Global earthquake locations are generally obtained by assuming an average crustal thickness of 30 km crust. However, the Tibetan Plateau crust is anomalously thick (60-75 km), so this assumption breaks down. Consequently earthquake locations reported within the Tibetan Plateau are likely in error. To investigate the size and impact of these errors on our estimates of P_n velocity, we have attempted to improve the locations of 16 local and regional earthquakes within the Tibetan Plateau. Mislocations can lead to large residuals in travel time curves, inaccurate fits, and consequently inaccurate measurements of mantle velocity and crustal thickness.

To explore the effects of epicenter mislocation on our estimates of P_n velocity, we used a simple grid search procedure to determine a new event epicenter and P_n velocity that best reduces the travel time residuals. The event epicenter is moved in a 1° by 1° grid, in 0.01° increments, centered about the initial PDE location. At each new latitude/longitude grid point, the new epicentral distances to each recording station and the travel times are fit with a new velocity. The grid point that produces the smallest mean error from the L1 fit is considered the new event location. Both origin time and focal depth are fixed in the relocation procedure because they will not have an effect on P_n velocity, only on the intercept time. Since we are interested in P_n velocity and event location obtained by minimizing residuals, the intercept time is not used. Adjustments to travel times for event origin time and focal depth corrections are common to all stations and would not reduce individual station residuals relative to the straight line fit. By fixing both origin time and focal depth and thereby travel time and only varying event location, we are analyzing relative travel times between recording stations. Finally, since we are fitting travel times across the plateau, we are assuming that a one-dimensional velocity structure is adequate and picking errors are small. No specific velocity structure is required so this technique allows us to explore the effects of event mislocation on the P_n velocity without the circularity of having to assume a particular velocity model (D. E. McNamara and W. R. Walter, Lithospheric structure of the Tibetan Plateau from relocation of local and regional earthquakes, submitted as UCID

at the Lawrence Livermore National Laboratory, Livermore, Calif., 1995).

From the 16 well-constrained new locations, relocation values ranged from just a few kilometers to as much as 34 km with a mean of 15 km. Individual event measurements of Pn velocity using the improved locations vary considerably (7.9-8.4 km/s). The large range of individual event Pn velocity estimates is an indication of lateral heterogeneity across the Plateau. Pn velocity from an individual event is biased by the individual event-station paths because of the small number of observations. Accurate determination of an average Pn velocity requires a large number of observations. Individual paths may be useful to characterize local variations in velocity structure.

Since travel time is fixed in our relocation procedure, the individual event intercept times no longer reflect the actual crustal travel time. After relocation, we normalize event travel times by removing the new intercept. By doing this we are able to combine every relocated event into one data set in order to compute an average Pn velocity for the region. From the 16 relocated events, 122 intercept normalized travel times are fit by a Pn velocity of 8.11 ± 0.14 km/s. With the original PDE locations, these same 122 arrivals are best fit by a velocity of

8.08 ± 0.18 km/s. Uncertainty is improved by only 0.04 km/s and the Pn velocity changes by only 0.37% suggesting that the average Pn velocity is relatively insensitive to event mislocations. Errors are averaged out when a large number of travel time observations are used. The velocities computed for this smaller data set are low relative to the entire plateau Pn data set. This is likely related to shorter path lengths and/or lateral velocity variations. These results suggest that a Pn velocity in the range of 8.1-8.2 km/s is an adequate average for the Tibetan Plateau and that a large number of arrivals should be used in the determination. Since we have minimized event location errors and shown that they do not significantly reduce scatter in our travel time data, it is reasonable to conclude that most of the scatter in Figure 2 is due to lateral variations in seismic velocity within the Tibetan Plateau.

S_n Propagation Characteristics

Data selection and frequency dependent amplitude measurement. Our objective is to infer lateral variations in upper mantle attenuation beneath the Tibetan Plateau by mapping lateral variations in S_n propagation efficiency as a function of

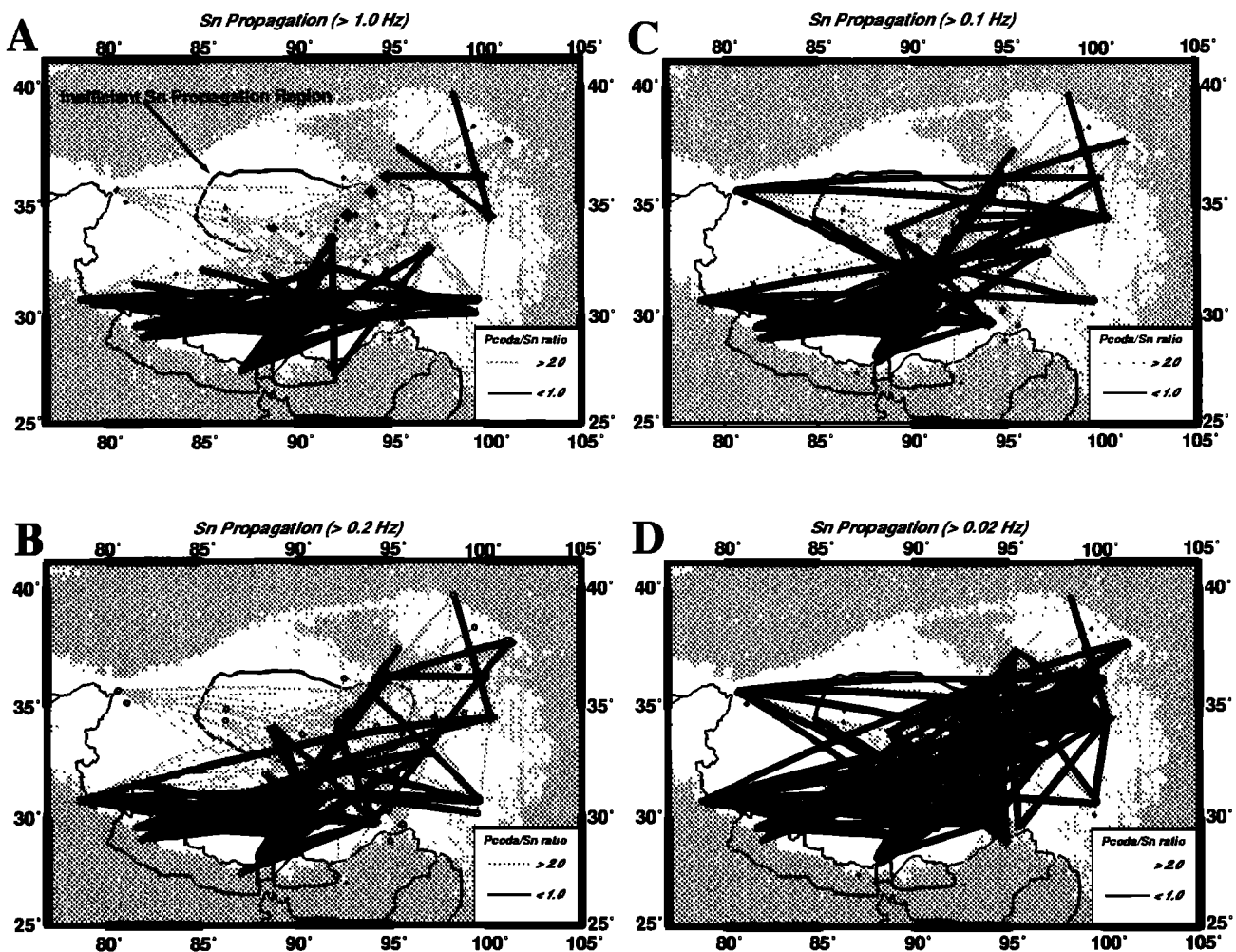


Figure 3. S_n propagation characteristics across the plateau shown for six frequency bands. The north central plateau is a previously identified region of inefficient S_n propagation [Barazangi and Ni, 1982]. Solid lines are paths with P coda/ S_n ratios less than 1.0. Grey lines are paths with P coda/ S_n ratios greater than 2.0. (a) S_n propagation greater than 1 Hz. (b) S_n propagation greater than 0.2 Hz. (c) S_n propagation greater than 0.1 Hz. (d) S_n propagation greater than 0.02 Hz.

frequency. Propagation efficiency is determined by measuring the amplitude of S_n relative to the P wave coda and can provide a qualitative measure of attenuation. The availability of numerous event/stations paths restricted to the Tibetan Plateau avoids any effect of the plateau boundaries on S_n amplitude and allows for detailed mapping of propagation efficiency. We also analyze events with locations outside of the Tibetan Plateau (Table 2). This second data set enables us to examine the effect that the plateau boundaries have on S_n propagation. By combining information from these two event data sets, we can avoid ambiguities of previous studies that have not benefited from multiple recording stations on the Tibetan Plateau [Ni and Barazangi, 1983].

We determined S_n propagation efficiency by comparing the maximum tangential amplitude of S_n to the average vertical amplitude of the P wave coda. For the measurement of amplitude, we first computed the envelope of the instrument corrected, displacement seismogram for both the high-pass-filtered tangential and vertical components of motion. We applied a high-pass, two-pole, two-pass, Butterworth filter at four different corner frequencies (1, 0.2, 0.1, and 0.02 Hz) to examine the effect of frequency content on S_n propagation efficiency. P coda amplitude was taken as the average amplitude on the vertical component within a window bounded by velocities of 8.0-5.0 km/s. S_n amplitude was taken as the maximum amplitude within a handpicked window bounding the time for waves traveling at our measured S_n velocity. When S_n was not observed at high frequencies, longer-period records were used. When no S_n energy was observed at long periods, amplitude was measured within a window bounded by 4.8 and 4.3 km/s. The long-period S_n picks were not used in velocity calculations since the exact arrival time is difficult to determine. After S_n amplitudes were determined relative to the P wave

coda, we examined individual event/station paths to search for a spatial pattern of S_n propagation efficiency.

Event/station paths were grouped by propagation efficiency which was determined by the P coda/ S_n ratio. In all cases, paths with P coda/ S_n ratios less than 1 were found to contain significant S_n energy, well above the average of the P coda. Paths with values from 1.0 to 1.5 often had weak S_n . However, a visual inspection was required for verification. In these cases, S_n was attenuated and often barely distinguishable from the P coda. Paths with values from 1.5 to 2.0 rarely had S_n energy distinguishable from the P coda. These were assumed to have severely attenuated S_n . Values greater than 2.0 were obtained when S_n was entirely absent from the seismogram.

Paths from events within and near the margins of the Tibetan Plateau are shown for four separate passbands in Figure 3. For clarity, we show only paths with strong S_n (P -coda/ $S_n \leq 1.0$) and no observed S_n (P -coda/ $S_n \geq 2.0$). From Figure 3a, it is apparent that at higher frequencies a greater number of paths do not have significant S_n energy. Strong high-frequency S_n is only observed for southern paths and paths north of the Kunlun fault (Figures 1 and 4), immediately verifying that our results are in agreement with a zone of inefficient high-frequency S_n propagation proposed by Ni and Barazangi [1983]. The density of our observations enable us to more precisely define the boundaries of this region. Specifically, we suggest that a larger portion of the northern plateau effectively blocks the propagation of high-frequency S_n . From paths shown in Figure 3a we observe that the original region of inefficient S_n propagation can be extended to the west and east, and we will verify this observation with specific examples (Figure 4).

To demonstrate the variable nature of high-frequency S_n propagation across the Tibetan Plateau, tangential component velocity record sections for five events are shown in Figures 5-

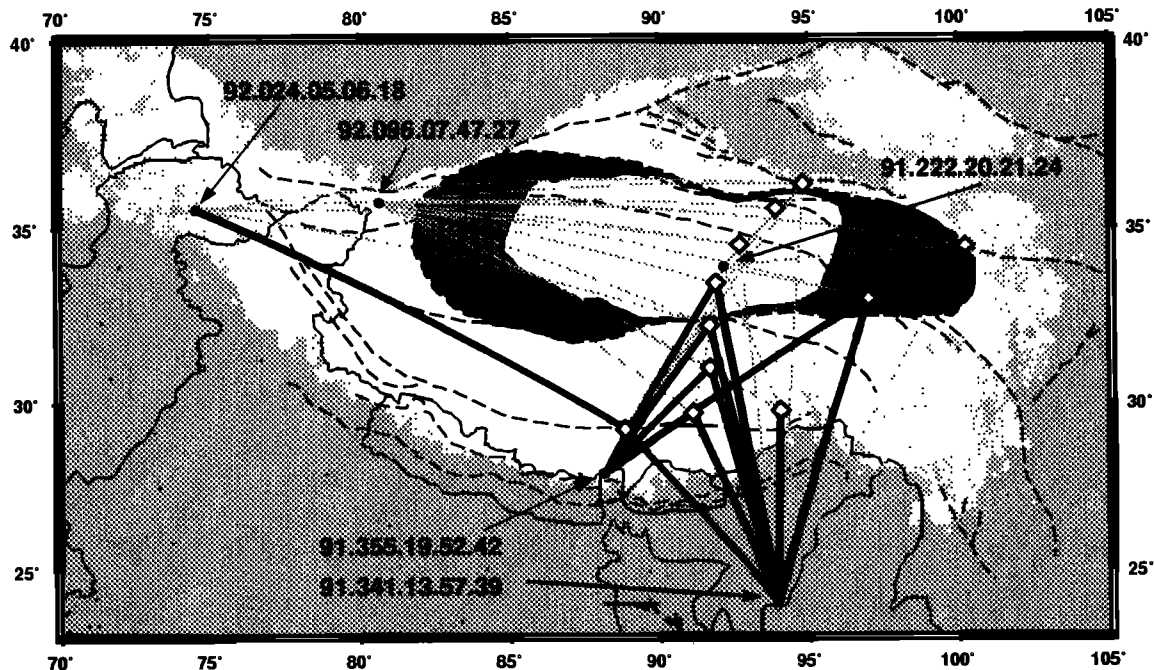


Figure 4. Examples of S_n propagation from five separate events. Solid lines show paths where S_n is observed. Grey lines show paths where S_n is not observed. The lightly shaded area is a region of high-frequency S_n attenuation, inferred from our data set. The open, inset, region is a previously identified zone of S_n attenuation. Also shown are our recording stations (diamonds) and the simplified regional structure of the Tibetan Plateau (dashed lines) [after Dewey et al., 1988].

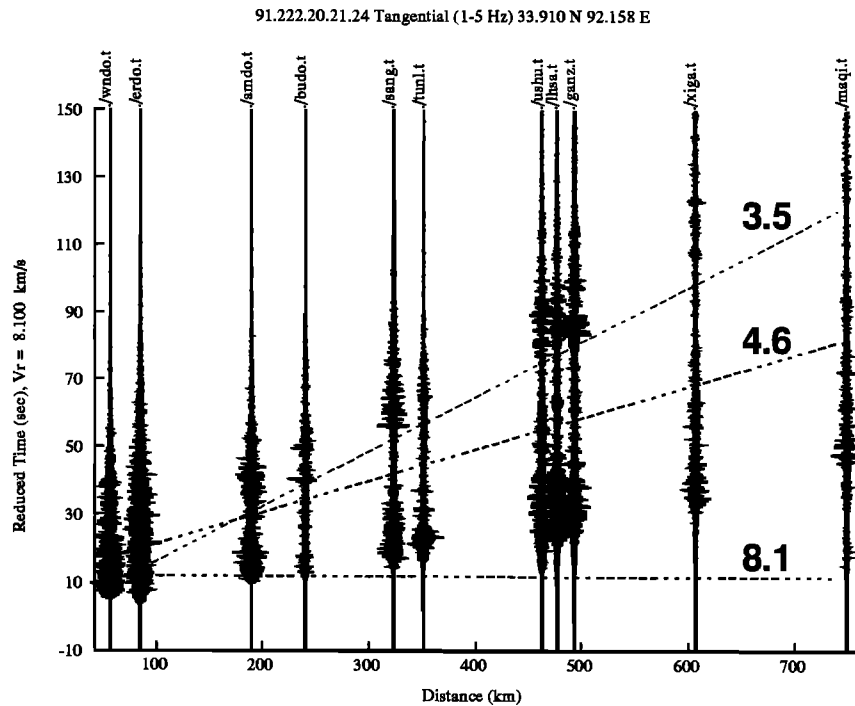


Figure 5. Central plateau local event record section (91.222.20.21.24). The tangential component of motion is shown band-pass-filtered (1-5 Hz) to simulate a short-period instrument, with the exception of LHSA. Data at LHSA was recorded continuously at a slower sampling rate of 5 samples/s. For this reason this trace is shown high pass filtered with a corner frequency of 0.5 Hz. Dashed lines show the approximate arrival times of P_n (8.1 km/s), S_n (4.6 km/s), and L_g (3.5 km/s).

9. Ray paths, for these events, are shown in Figure 4. Each record section is shown with a reducing velocity of 8.1 km/s an S_n travel time prediction, based on the observed S_n velocity and intercept time, and the predicted L_g arrival time for a velocity of 3.5 km/s. A two-pole, two-pass, band-pass, Butterworth filter with corner frequencies of 1 and 5 Hz was applied to suppress large-amplitude surface waves. Each seismogram is scaled to peak amplitude to facilitate visual comparison of the traces.

Event 91.222.20.21.24 (Figure 5) occurred within the region of inefficient S_n propagation proposed by Ni and Barazangi [1983] and shows no significant high-frequency S_n energy. This event was recorded by all eleven stations, covering an azimuthal range of nearly 180° (Figure 4). Source radiation pattern alone would not eliminate S_n at all stations throughout a such large range of azimuths. Instead, S_n is likely attenuated, along the travel path, before it reaches the recording stations. Event 91.355.19.52.42 (Figure 6), located in southern Tibet (Figure 4), shows S_n propagating to southern stations (XIGA, LHSA, SANG, AMDO, WNDO, and USHU) and weak to nonexistent at northern stations (MAQI, ERDO, BUDO, and TUNL). Note the gradual, northward, decrease in S_n amplitude and frequency content from AMDO, through WNDO to ERDO over a roughly 200-km path length. This suggests that the southern boundary of the zone of inefficient S_n propagation is transitional and in this case allows some S_n energy to reach WNDO. However, energy quickly dies out as evidenced by the lack of S_n at ERDO and BUDO (Figure 6). Note also the dramatic S_n energy decrease along the same azimuth from USHU to MAQI. Source radiation pattern alone could not account for S_n blockage along a common azimuth. Significant

changes in upper mantle properties must exist between USHU and MAQI indicating that the region of high-frequency inefficient S_n propagation must extend eastward.

The western boundary of the zone of inefficient S_n propagation can also be verified and mapped in more detail with our data set. For example, note the complete absence of S_n in event 92.096.07.47.27 (Figure 7) from the western Tibetan Plateau. Southern stations (GANZ, SANG, and LHSA) have no apparent S_n energy suggesting the zone of inefficient S_n propagation may extend farther to the west than previously suggested. Azimuthal coverage is limited so source radiation pattern could possibly explain the lack of observable S_n for this event. However, several events from the same region show similar weak to nonexistent S_n at all recording stations, suggesting that this effect is more likely due to attenuation along the path rather than source radiation (Figure 3a).

High-frequency S_n propagation from events outside the Tibetan Plateau. We have included additional events, with source locations outside of the plateau to add further constraints to the spatial distribution of high-frequency S_n propagation. The most significant observation from this data set is that the southern boundary of the Tibetan Plateau has little to no effect on the propagation of S_n . Event 91.341.13.57.39, from directly south of the plateau (Figures 8 and 4) demonstrates that the structures beneath the Himalaya mountain range do not adversely affect S_n propagation. S_n clearly arrives at all stations in the southern portion of the array but is absent at stations to the north. Again a rapid energy decrease occurs as S_n propagates from WNDO to ERDO and from USHU to MAQI. Similar propagation characteristics are observed for event 91.355.19.52.42 (Figure 6) and can be used to constrain the

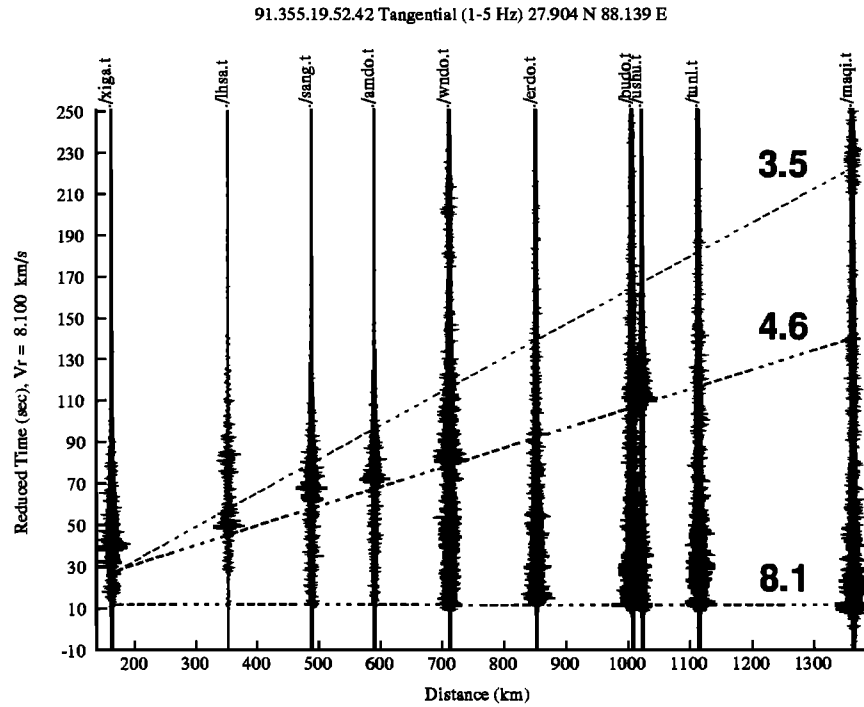


Figure 6. Southern plateau local event record section (91.355.19.52.42). Display parameters are the same as Figure 5.

southern and eastern boundaries of inefficient high-frequency *Sn* propagation. Specifically, the southern boundary, proposed by [Ni and Barazangi [1983], is along the Bangong-Nujiang suture (Figure 1), but the eastern boundary must be extended between USHU and MAQI. Also, note the early arrival of *Pn* relative to the reducing velocity of 8.1 km/s (Figure 6). The velocity for this single event is fast (8.3 km/s) and is likely due

to a large portion of these paths traveling within the faster mantle lid beneath India.

Event 92.024.05.06.18, from the west in Pakistan (Figures 9 and 4), can be used in conjunction with event 92.096.07.47.27 (Figure 7) to help better define the western boundary of *Sn* attenuation. Note the strong *Sn* arrival at XIGA and its absence at AMDO (Figure 9). This observation provides evidence for

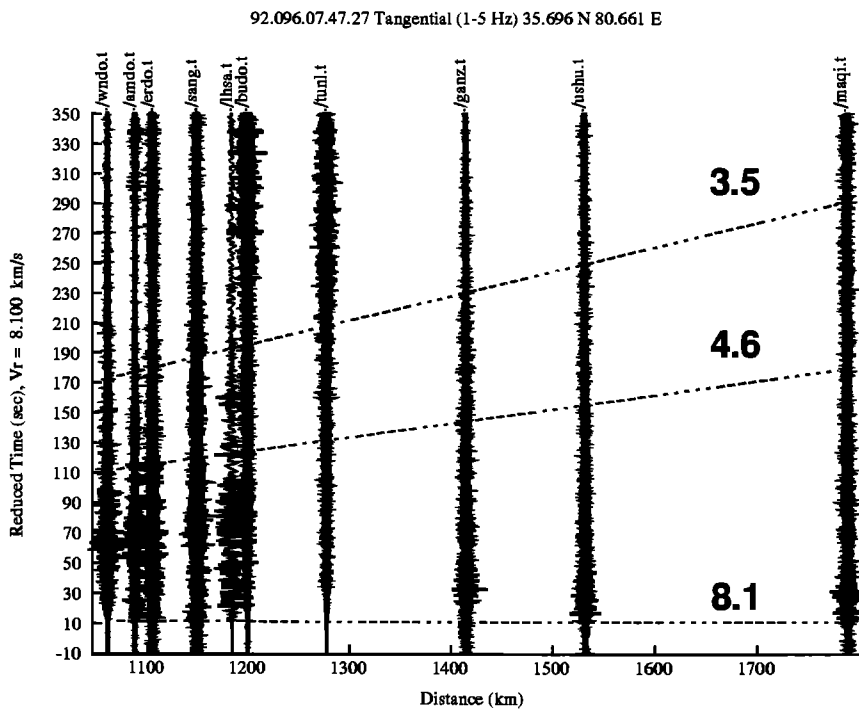


Figure 7. Regional event record section from the northwestern Tibetan Plateau (92.096.07.47.27). Display parameters are the same as Figure 5.

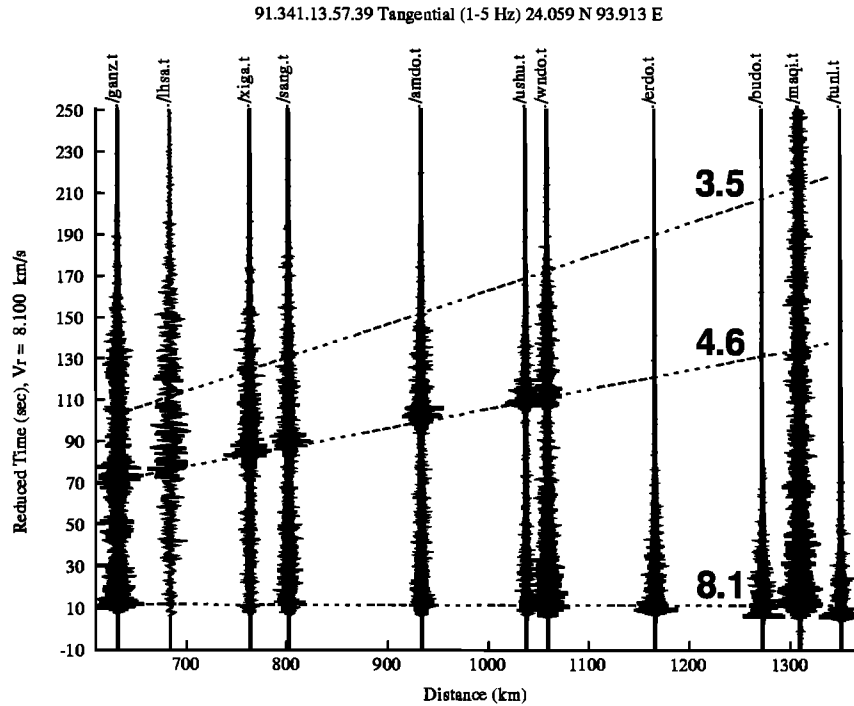


Figure 8. Regional record section from a Burmese event, southeast of the Tibetan Plateau (91.341.13.57.39). Display parameters are the same as Figure 5.

the maximum westward extent of the zone of inefficient, high-frequency, *Sn* propagation. It cannot extend past the path from event 91.024.05.06.18 to the station XIGA (Figure 4). Our data set has limited ability to constrain the western boundary; however, [Ni and Barazangi [1983] observed efficient *Sn* propagation in the westernmost Tibetan Plateau. Events, west of 82°E in the vicinity of event 92.096.07.46.27, had observable *Sn* energy propagated to recording stations to the south and west of

the plateau. *Sn* was not observed at stations to the southeast. Based on the combination of our data set with previous observations, we limit the westward expansion of the region of inefficient *Sn* propagation to about 82°E (Figure 4).

Shear wave energy is observed passing through the northern plateau for event 92.024.05.06.18 at USHU (Figure 9). Since the epicentral distance is beyond 1800 km, this arrival is not *Sn*. It is, instead, shear wave energy that travels deeper in the

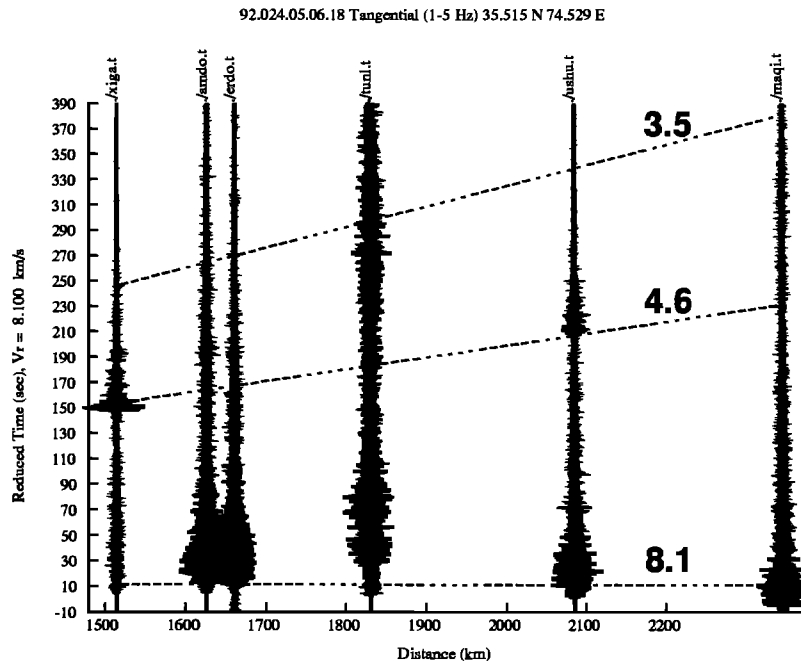


Figure 9. Regional event record section from Pakistan, west of the Tibetan Plateau (92.024.05.06.18). Display parameters are the same as Figure 5.

sublithospheric mantle and propagates efficiently even beneath the north central portion of the plateau. This would suggest that the mechanism affecting S_n propagation is contained within the lithospheric portion of the mantle.

The northern and southern boundaries of inefficient S_n propagation appear to coincide with regional structural trends. We observe strong high-frequency S_n for three paths north of the Kunlun Range, recorded at TUNL and MAQI (Figure 3a). This supports the idea that the northern boundary is coincident with the Kunlun front, as previously suggested by [Ni and Barazangi [1983]. Based on the number of paths with no observable high-frequency S_n arrivals from west central plateau events at central plateau stations (AMDO, WNDO and SANG), we suggest that the southern boundary coincides with the Banggong-Nujiang suture (Figures 1 and 4). The remaining boundaries can be refined based on our new observations and appear to closely follow regional structural trends in the northern plateau (Figure 4).

Frequency dependent S_n propagation across the Tibetan Plateau. We have shown that for frequencies greater than 0.5 Hz, S_n is severely attenuated in the northern portion of the Tibetan Plateau (Figure 3a). When slightly longer periods are included in the analysis, up to 5-10 s (0.2-0.1 Hz), S_n energy is observed, crossing through the northern plateau, for long paths and when only a small portion of the path (<200 km) enters the northern plateau (Figures 3b and 3c). With further increasing period, the number of paths with P coda/ S_n ratios less than one (strong S_n) increases, while paths with P coda/ S_n ratios greater than two (no S_n) decreases (Figure 3d). These observations indicate that S_n propagation is frequency dependent and that in general S_n propagation efficiency decreases with increasing frequency. High-frequency S_n is severely attenuated as it propagates throughout the northern plateau, but S_n at longer periods is able to propagate throughout the entire plateau.

Discussion

Upper mantle velocity structure beneath the Tibetan Plateau. Regional P_n and S_n velocities are commonly used to investigate the nature of the uppermost mantle because they can vary greatly between stable shield and tectonically active regions [Molnar and Oliver, 1969; Cormier, 1982]. The average P_n velocity beneath continents is 8.1 km/s [Mooney and Braile, 1989]. Stable cratonic shields are generally faster. For example, P_n and S_n propagate with velocities of 8.4 and 4.5 km/s, respectively, beneath the Indian Shield [Ni and Barazangi, 1983]. Relatively slower P_n and S_n velocities as well as high attenuation are typical of regions with active tectonics [Beghoul et al., 1993; Cormier, 1982; A. J. Rodgers et al., P_n , S_n and L_g propagation in the Middle East, submitted to the *Bulletin of the Seismological Society of America*, 1995]. For example, P_n velocity measured in the tectonically active Basin and Range Province is as low as 7.8 km/s, and S_n has been shown to propagate inefficiently [Beghoul et al., 1993; Benz et al., 1990]. A similar relationship between low P_n velocity (7.7 km/s) and inefficient S_n propagation has been observed beneath the Turkish-Iranian Plateau (A. J. Rodgers et al., submitted manuscript, 1995).

With these relationships in mind, the velocity and propagation characteristics of P_n and S_n have been used to place constraints on the evolution of convergence between the Indian and Eurasian lithospheric plates. Despite the currently active tec-

tonics within the plateau, our P_n and S_n velocities are typical for continental paths and roughly in the middle of values observed from previous studies. The apparently "typical" values are likely caused by the doubly thick overlying crust. Molnar [1988] argued that an increase in pressure within the upper mantle beneath the Tibetan Plateau, due to a 70-km-thick overlying crust, could increase the P_n velocity by as much as 0.15 km/s relative to P_n beneath an average crust (40 km). Applying this correction decreases our observed P_n velocity to about 8.0 km/s. This lower value is more typical of a tectonically active region and well below a P_n velocity expected if the Indian Shield is underthrust beneath the Tibetan Plateau. However, 8.0 km/s is still significantly higher than P_n velocities beneath the Basin and Range and the Turkish-Iranian Plateau, where strong S_n attenuation is also observed.

Mantle variations across the Tibetan Plateau. The region of inefficient high-frequency S_n propagation, delineated here, extends the zone previously reported by Ni and Barazangi [1983] to include a larger portion of northern Tibetan Plateau (Figure 4). We have also verified that P_n velocity, for paths restricted to this region of inefficient S_n propagation in the north, is approximately 4% slower than the velocity measured using only southern plateau paths. Low P_n velocity coincident with inefficient S_n propagation has been observed beneath the Turkish-Iranian Plateau and the Basin and Range Province of North America [Rodgers et al., 1995; Beghoul et al., 1993]. Rodgers et al. [1995] argue that partial melt within the mantle lid is a possible cause of this type for inefficient S_n propagation.

The north central Tibetan Plateau is particularly interesting because of the large amount of seismic data that can be interpreted as evidence for high temperatures within the uppermost mantle relative to the southern plateau. For example, in addition to the results presented here, previous studies have reported observations of large teleseismic S - P travel time residuals [Molnar and Chen, 1984; Molnar, 1990], slow regional shear wave propagation to a depth of 250 km [Lyon-Caen, 1986] slow Rayleigh wave group velocities [Brandon and Romanowicz, 1986], slow P_n velocities [Zhao and Xie 1993; Holt and Wallace 1990], and large values of shear wave splitting [McNamara et al., 1994]. The seismic evidence is corroborated by surface geology. In the northern Tibetan Plateau there is strong evidence for widespread Cenozoic volcanism with both basaltic and granitic components [Deng, 1978; Dewey et al., 1988; Burke et al., 1974; Molnar, 1988]. The basaltic component suggests volcanic sources are from partial melt of upper mantle material.

Gajewski et al. [1990] computed regional distance reflectivity synthetic seismograms, tested several different models, and concluded that a depth increasing V_p/V_s is the likely cause of weakened S_n in the presence of P_n . It is difficult to explain decreasing V_p/V_s with attenuation, temperature, and pressure effects alone since each would affect both the P and S wave gradients nearly equally. In a study similar to that of [Gajewski et al. [1990], Crotwell et al. [1995] model events common to this study and show that Q_s levels low enough to suppress high-frequency S_n also significantly attenuate P_n . They showed that rather than low Q , different P and S wave velocity gradients can decrease high-frequency S_n amplitudes while allowing longer-period energy to propagate relatively efficiently. In the future, these models may aid in quantifying the mechanism of P_n and S_n frequency dependent attenuation within the plateau. Our existing qualitative attenuation infor-

mation does, however, allow some speculation. Based on the modeling of *Crotwell et al.* [1995] and *Gajewski et al.* [1990], we should not observe Pn if attenuation is sufficient to suppress Sn . We do, however, observe high-frequency Pn propagating throughout the region of inefficient Sn propagation in the northern plateau. By eliminating simple attenuation, we require an alternative explanation for the propagation characteristics observed in our regional data set.

Variations in upper mantle temperature are generally considered to be the dominant mechanism responsible for lateral Pn velocity variations. [*Hearn et al.* 1991; *Black and Braile* 1982]. We have argued, however, that temperature alone cannot cause inefficient Sn propagation in the presence of Pn . Instead, we suggest that compositional effects within the uppermost mantle as a function of lateral temperature variations are responsible for both observations from our regional phase propagation data set. *Fuchs* [1983] has shown that a gradual increase in olivine content, relative to orthopyroxene and clinopyroxene, with depth due to the depletion of basalt within the uppermost mantle, would cause a depth-increasing Vp/Vs ratio. In this case, a relatively weaker shear wave gradient would not generate significant Sn energy, while the stronger, compressional wave gradient propagates Pn energy. Such a mechanism can explain both inefficient Sn propagation and low Pn velocity.

Geologic observations from the northern plateau are consistent with the idea that inefficient Sn propagation is related to partial melt of the lithospheric mantle. Young basaltic volcanism is observed in the northern plateau and is indicative of partial melt from an upper mantle source. Progressive basalt depletion with depth would enrich the upper mantle in olivine and generate a depth-increasing Vp/Vs ratio. Additional broadband waveform modeling and composition-based modeling is required to precisely define the upper mantle velocity gradients beneath the northern plateau. However, at this point, we are able to argue that a depth-increasing Vp/Vs ratio, due to partial melt of the uppermost mantle, is a plausible model to explain the propagation characteristics that we observe in our regional data set.

Tectonic implications. From the observed lateral heterogeneity in our data we can infer lateral temperature and compositional variations within the upper most mantle across the plateau. These are significant constraints that models describing the evolution of the collision between the Indian and Eurasian plates must address. Such lateral heterogeneity in the deep structure is not initially expected, due to uniform topography across the plateau, and suggests that complex mechanisms of isostatic compensation are involved. Most tectonic models attribute the characteristics of the Tibetan Plateau to some combination of underthrusting of the Indian lithosphere beneath the southern margin of Eurasia, distributed shortening and thickening of the Eurasian lithosphere and lateral extrusion of crustal blocks. Each existing model has limitations, but all may play a role in some aspect of plateau evolution. As analysis of data from our experiment and other recent studies on the area continue, the improved the resolution of anomalies beneath the region should allow refinement of models describing the evolution of this important continental collision.

Conclusions

We have presented observations of regional seismic wave propagation within the Tibetan Plateau that has enabled us to better define the deep velocity and attenuation structure. The

coverage provided by our temporary deployment allows us to analyze a large number of propagation paths confined to the plateau interior for the first time. Using these data, we are able to demonstrate lateral variations in crustal thickness, Pn velocity and Sn propagation efficiency. We have observed an average crustal thickness of approximately 65 km that thins from the south (57 km) to the north (69 km). We have also determined an average Pn velocity of 8.16 ± 0.07 km/s and have shown that the northern plateau is 4% slow relative to the southern plateau. The average velocity is high relative to tectonically active regions but is in the middle range of published Tibetan Plateau Pn velocities. If pressure and velocity gradient corrections were considered, the Pn velocity would be comparable to tectonically active areas with normal crustal thickness. Despite the path restrictions and attempts to improve event locations, the scatter of Pn travel times remains large, indicating velocity heterogeneity within the plateau. Further characterization of this heterogeneity may be possible through tomographic analysis of our Pn travel times as well as waveform modeling of individual station-event paths.

We have also shown that Sn propagation amplitude across the Tibetan Plateau is frequency dependent. The Sn velocity estimate determined in this study is high relative to other tectonically active regions but is biased by the complete lack of measurable Sn arrivals in the northern portion of the plateau. High-frequency Sn is severely attenuated throughout the entire northern plateau, extending a zone of inefficient Sn propagation previously identified in the north central plateau [*Barazangi and Ni*, 1982; *Ni and Barazangi*, 1983]. Observations of crustal shear waves and shear waves at greater distances propagating through this zone suggests that the mechanism impeding Sn propagation is confined to the uppermost mantle within the northern plateau. Our results require first-order variations in the uppermost mantle structure, despite the relatively uniform topography of the Tibetan Plateau.

Acknowledgments. The authors would like to thank the many scientists and field workers who endured the hardships of the Tibetan Plateau and greatly contributed to the success of this experiment. We would especially like to thank Frances Wu, whose persistence made this cooperative effort possible. Contributors included Chinese participants from the Institute of Geophysics, State Seismological Bureau, PRC, and the Seismological Bureaus of the Qinghai Province and the Tibetan Autonomous Region. U.S. participants in the field program included F. Wu (SUNY-Binghamton), R. Busby (PIC-LDGO), R. Kuehnel (Carnegie-DTM), G. Randall, G. Wagner, S. Owens and M. Salvador (USC). This project was supported by NSF grants EAR-9004428, EAR-9196115 and EAR-9206815 to USC. Event relocation work was supported by LLNL in the summer of 1993 and performed under the auspices of the U.S. Department of Energy by Lawrence Livermore National Laboratory under contract W-7405-ENG-48. G. Randall provided insight on regional phase propagation, and comments from M. Barazangi, W. Holt, and D. James helped improve our presentation and interpretation.

References

- Argand, E., La tectonique de L'Asie, *Proc. 13th Geol. Cong. Brussels*, 13, 170-372, 1924.
- Barazangi, M., and J. Ni, Velocities and propagation characteristics of Pn and Sn beneath the Himalayan arc and Tibetan Plateau: Possible evidence for underthrusting of Indian continental lithosphere beneath Tibet, *Geology*, 10, 179-185, 1982.

- Beckers, J., S. Y. Schwartz, and T. Lay, The velocity of the crust and upper mantle under China from broadband *P* and *PP* waveform analysis, *Geophys. J. Int.*, **119**, 574–594, 1994.
- Beghoul, N., M. Barazangi, and B. L. Isacks, Lithospheric structure of Tibet and western North America: Mechanisms of uplift and a comparative study, *J. Geophys. Res.*, **98**, 1997–2016, 1993.
- Benz, H. M., R. B. Smith, and W. D. Mooney, Crustal structure of the northwest Basin and Range province from the 1986 program for array seismic studies of the continental lithosphere seismic experiment, *J. Geophys. Res.*, **95**, 21,823–21,842, 1990.
- Black, P. R., and L. W. Braile, *Ps* velocity and cooling of the continental lithosphere, *J. Geophys. Res.*, **87**, 10,557–10,568, 1982.
- Brandon, C., and A. Romanowicz, A "no-lid" zone in the central Chang-Thang platform of Tibet: Evidence from pure path phase velocity measurements of long-period Rayleigh waves, *J. Geophys. Res.*, **91**, 6547–6564, 1986.
- Burke, K. C., J. F. Dewey, and W. S. Kidd, The Tibetan Plateau: Its significance for tectonics and petrology, *Geol. Soc. Am. Abstr. Programs.*, **6**, 1027–1028, 1974.
- Chen, W. P., and P. Molnar, Constraints on seismic wave velocity structure beneath the Tibetan Plateau and their tectonic implications, *J. Geophys. Res.*, **86**, 5937–5962, 1981.
- Cormier, V. F., The effect of attenuation on seismic body waves, *Bull. Seismol. Soc. Am.*, **72**, S169–S200, 1982.
- Crotwell, P., G. R. Randall, D. E. McNamara, and T. J. Owens, Frequency-dependent propagation of regional *Sn* within the Tibetan Plateau, *Eos Trans. AGU*, **76** (17), Spring Meet. Suppl., S201, 1995.
- Deng, W., A preliminary study on the petrology and petrochemistry of the Quaternary volcanic rocks of the northern Tibet autonomous region, *Acta Geol. Sin., Engl. Transl.*, **52**, 148–152, 1978.
- Dewey, J. F., and K. C. A. Burke, Tibetan Variscan, and Precambrian basement reactivation: Products of continental collision, *J. Geol.*, **81**, 683–692, 1973.
- Dewey, J. F., R. M. Shackleton, F. R. S. C. Cheng, and S. Yiyin, The tectonic evolution of the Tibetan Plateau, *Philos. Trans. R. Soc. London.*, **327**, 379–413, 1988.
- Ding, Z., R. Zeng, and F. T. Wu, The *Pn* wave velocities and the relief of Moho in the Tibetan Plateau, *Acta Seismol. Sin.*, **6**, 317–325, 1993.
- Fuchs, K., Recently formed elastic anisotropy and petrological models for the continental subcrustal lithosphere in southern Germany, *Phys. Earth Planet. Inter.*, **31**, 93–118, 1983.
- Gajewski, D., R. Stangl, K. Fuchs, and K. J. Sandmeier, A new constraint on the composition of the topmost continental mantle-anomalously different depth increases of *P* and *S* velocity, *Geophys. J. Int.*, **103**, 497–507, 1990.
- Harrison, T. M., P. Copeland, W. S. F. Kidd, and A. Yin, Raising Tibet, *Science*, **255**, 1663–1670, 1992.
- Hearn, T. M., N. Beghoul, and M. Barazangi, Tomography of the western United States from regional arrival times, *J. Geophys. Res.*, **96**, 16,369–16,381, 1991.
- Holt, W. E., and T. C. Wallace, Crustal thickness and upper mantle velocities in the Tibetan Plateau region from the inversion of regional *Pnl* waveforms: Evidence for a thick upper mantle lid beneath southern Tibet, *J. Geophys. Res.*, **95**, 12,499–12,525, 1990.
- Jia, S., X. Cao, and J. Jia, The *P* wave travel times and upper mantle structure of the Tibetan Plateau, *N. West. Seism. J.*, **3**, 27–34, 1981.
- Lyon-Caen, H., Comparison of the upper mantle shear wave velocity structure of the Indian shield and the Tibetan Plateau and tectonic implication, *Geophys. J. R. Astron. Soc.*, **86**, 727–749, 1986.
- McNamara, D. E., T. J. Owens, P. G. Silver, and F. T. Wu, Shear wave anisotropy beneath the Tibetan Plateau, *J. Geophys. Res.*, **99**, 13,655–13,665, 1994.
- Molnar, P., A review of geophysical constraints on the deep structure of the Tibetan Plateau, the Himalaya and the Karakoram, and their tectonic implications, *Trans. R. Soc. London*, **A327**, 33–88, 1988.
- Molnar, P., *S*-wave residuals from earthquakes in the Tibetan region and lateral variations in the upper mantle, *Earth Planet. Sci. Lett.*, **101**, 68–77, 1990.
- Molnar, P., and J. Oliver, Lateral variations of attenuation in the mantle and discontinuities in the lithosphere, *J. Geophys. Res.*, **74**, 2648–2682, 1969.
- Molnar, P., and W. P. Chen, *S-P* travel time residuals and lateral inhomogeneity in the mantle beneath Tibet and the Himalaya, *J. Geophys. Res.*, **89**, 6911–6917, 1984.
- Mooney, W. D., and L. W. Braile, The seismic structure of the continental crust and upper mantle of North America, in *The Geology of North America-An Overview*, edited by A. W. Bally and A. R. Palmer, Geol. Soc. of Am., Boulder, Colo., v. A, pp. 39–52, 1989.
- Ni, J., and M. Barazangi, High frequency seismic wave propagation beneath the Indian shield, Himalayan arc, Tibetan Plateau and surrounding regions: High uppermost mantle velocities and efficient propagation beneath Tibet, *Geophys. J. R. Astron. Soc.*, **72**, 665–689, 1983.
- Owens, T. J., G. E. Randall, F. T. Wu, and R. S. Zeng, PASSCAL instrument performance during the Tibetan Plateau passive seismic experiment, *Bull. Seismol. Soc. Am.*, **83**, 1959–1970, 1993a.
- Owens, T. J., G. E. Randall, D. E. McNamara, and F. T. Wu, Data report for the 1991–92 Tibetan Plateau passive-source seismic experiment, *PASSCAL Data Rep. 93-005*, IRIS, Wash. D.C., 1993b.
- Zhao, L. S., and D. V. Helmberger, Geophysical Implications from relocations of Tibetan earthquakes: Hot lithosphere, *Geophys. Res. Lett.*, **18**, 2205–2208, 1991.
- Zhao, L. S., and J. Xie, Lateral variations in compressional velocities beneath the Tibetan Plateau from *Pn* traveltimes tomography, *Geophys. J. Int.*, **115**, 1070–1084, 1993.

D. E. McNamara and W. R. Walter Earth Sciences Division, Lawrence Livermore National Lab., P.O. Box 808, L-202, Livermore, CA 94551 (e-mail: mcnamara3@llnl.gov).

T. J. Owens, Department of Geological Sciences, University of South Carolina, Columbia, SC 29208.

(Received October 4, 1994; revised April 20, 1995; accepted June 6, 1995.)